www.MaterialsViews.com

ADVANCED
OPTICAL
MATERIALS
www.advopticalmat.de

COMMUNICATION

Manipulation of Asymmetric Transmission in Planar Chiral Nanostructures by Anisotropic Loss

Zhaofeng Li, Mutlu Gokkavas, and Ekmel Ozbay**

Nonreciprocal transmission plays a fundamental role in information processing. Stimulated by the successful application of the electrical diode that shows nonreciprocal response in electric circuits, considerable effort has been devoted to the study of nonreciprocal propagation of light. One way of achieving nonreciprocity in optics is to use a magneto-optical medium that breaks the time-reversal symmetry by introducing a set of antisymmetric, off-diagonal dielectric tensor elements.[1] The other way is to use a nonlinear medium.[2,3] Apart from thes two conventional methods, it has been demonstrated that nonreciprocal light propagation can be realized by the breaking of parity-time symmetry with complex optical potentials.[4,5] The main idea of the above implementations is to make the light propagate through the media in different manners for opposite propagation directions. Meanwhile, there were attempts to achieve asymmetric but still reciprocal transmission by using conventionally isotropic, linear, and lossy or lossless materials. For instance, the asymmetric transmission of linearly polarized waves can be realized by using diffractive nonsymmetrical volumetric gratings based on photonic crystals or metals,[6] using nonsymmetrical two layered metallic structures,[7] using nonsymmetrical metallic gratings supporting surface plasmons,[8] and using dielectric gratings.[9] The asymmetric transmission of circularly polarized waves has been demonstrated at normal incidence by using a multilayered structure[7,10] and by using a planar chiral structure (PCS) consisting of single layer of metaatoms.[11–17] For many of these structures,[7,9–17] asymmetric transmissions are realized due to the different transmissions in the cross-polarized components, while the transmissions of co-polarized components remain the same because of the reciprocity of the materials. Among these structures, the PCS is a special one. First, it is a simple, two-dimensional planar structure that is easy to fabricate. Second, in contrast to a three-dimensional structure in which loss is not an important factor for the realization of asymmetric transmission,[7] a PCS must be simultaneously anisotropic and lossy to achieve the asymmetric transmission of circularly polarized waves. Although many of the previous reports have studied the influence of anisotropy of the geometric structures on the asymmetric transmission realized in PCSs,[11–17] the influence of loss was only mentioned empirically or qualitatively and was far from clarified.

Dr. Z. Li, Prof. M. Gokkavas, Prof. E. Ozbay
Department of Electrical and Electronics Engineering
Department of Physics
Nanotechnology Research Center
Bilkent University, Bilkent
06800, Ankara, Turkey
E-mail: zhaofengli@bilkent.edu.tr; ozbay@bilkent.edu.tr

Here, we study a typical PCS composed of two sets of gold split ring resonators (SRRs), and analyze the mechanism of asymmetric transmission by using an optical lumped element (OLE) model. We have obtained, for the first time, a formula that quantitatively relates the asymmetric transmission to the factor of loss and, more strikingly, we find that it is the anisotropy of loss, instead of the whole loss, that is crucial for achieving the asymmetric transmission. According to the formula, we demonstrate numerically and experimentally that the asymmetric transmission can be manipulated by changing the anisotropy of loss.

Figure 1a shows the schematics of the PCS under study. It is composed of two sets of gold SRRs with different sizes arranged periodically in a square lattice. Contrastingly, all of the PCSs reported previously were composed of SRRs with the same dimension.[18–20] The SRRs stand freely in vacuum (or air). In accordance with the definition of a PCS, the whole structure cannot be superimposed on its in-plane mirror image (reflected by a mirror perpendicular to the plane of the structure) unless it is lifted from the plane.[11–13] The periodic constants of the PCS in the lateral directions are $a_x = a_y = 540$ nm and, therefore, the structure does not diffract the incident light wave with operation wavelengths ranging from 1.0 μm to 2.0 μm in the present study. The thickness of the gold wires is 50 nm, which is much smaller than the operation wavelength so that the structure can be seen as a planar metamaterial for normally incident light waves.

SRRs are popular building blocks of metamaterials and have been studied intensively.[21–24] The low-frequency resonance of SRRs can be well modeled by series resistor–inductor–capacitor (RLC) circuits at infrared and lower frequencies.[22,25] There exists a coupling effect between the SRRs oriented in the x and y directions around resonant frequencies.[18–20] The RLC resonance of an individual SRR[22] mainly consists of a magnetic dipole (μ) in the direction that is normal to the plane of the SRR and an electric dipole (p) along the direction of the gap of the SRR,[25,26] as indicated in Figure 1b. Since the electric dipoles of the SRRs oriented in the x and y directions are perpendicular to each other, there is no coupling effect between them. On the other hand, the magnetic dipoles of all the SRRs are in the same direction (z direction) and, therefore, they can couple to each other magnetically. By treating all the resonators as a whole metafilm and combining it with transmission line theory, circuit models with lumped element parameters have been successfully used to analyze metamaterials working at terahertz and infrared regions.[27,28] Here, we also use an OLE model to describe the infrared light wave propagation through the PCSs.

In Figure 1a, when a right-circularly polarized (RCP, +) wave or a left-circularly polarized (LCP, −) wave is incident in the +z direction, the transmitted wave will possess both RCP and LCP

ADVANCED
OPTICAL
MATERIALS
www.advopticalmat.de

Materials
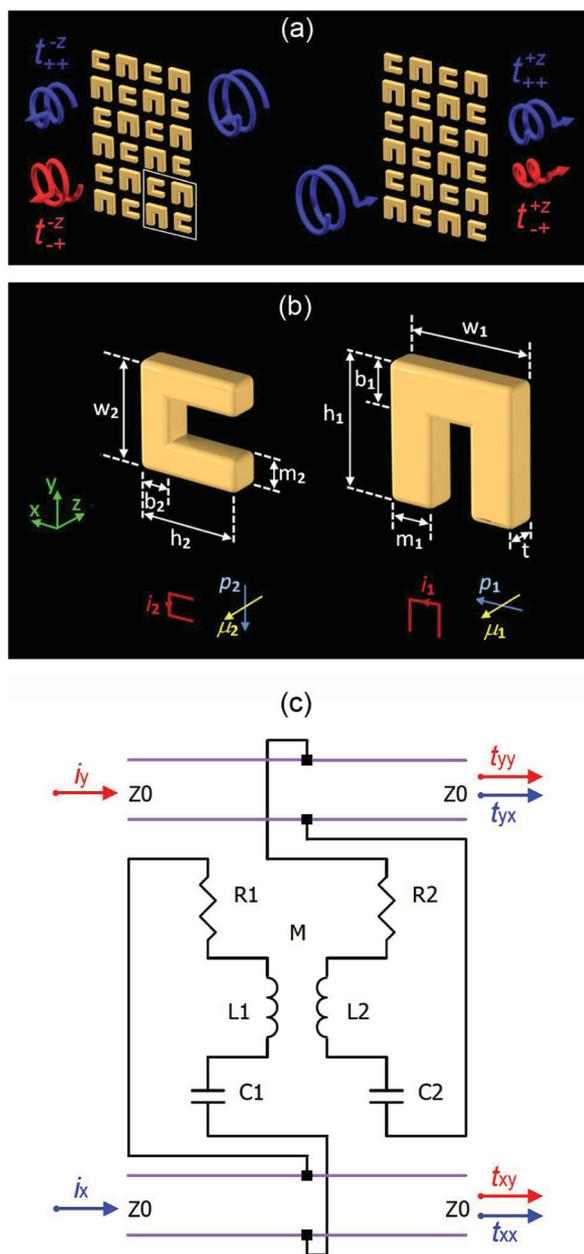Views
www.MaterialsViews.com

COMMUNICATION

Figure 1. (a) Schematics of the planar chiral structure under normal incidence of right-circularly polarized light waves. A unit cell is marked with white box. The periodic constants in the x and y directions are $a_x = a_y = 540$ nm. (b) The definitions of the geometrical parameters for the two different SRRs used in this article. The bottom of (b) shows the electric and magnetic dipoles corresponding to the RLC resonance of the SRRs. (c) The optical lumped element model corresponding to the planar chiral structure of (a).

While the Lorentz Reciprocity Lemma requires that $t_{\pm\pm}^{+z} = t_{\pm\pm}^{-z}$ and $t_{\mp\pm}^{+z} = t_{\pm\mp}^{-z}$, it does not restrict the relative values of $t_{\mp\pm}^{+z}$ and $t_{\mp\pm}^{-z}$. If $\left|t_{-+}^{+z}\right|^2 \neq \left|t_{-+}^{-z}\right|^2$, then $\Delta_+ = T_+^{+z} - T_+^{-z} = \left|t_{-+}^{+z}\right|^2 - \left|t_{-+}^{-z}\right|^2$ is a nonzero value, which means an asymmetric transmission for RCP waves traveling in the +z and −z directions. At the same time, for LCP waves, the asymmetric transmission is just the opposite of RCP waves, $\Delta_- = -\Delta_+$. For the purpose of clearness and conciseness, in the present report, we will only consider the case of RCP waves.

Figure 1c shows the equivalent OLE model for the PCS of Figure 1a. In the model, the two sets of SRRs are described by two coupled, lumped-element RLC oscillators behaving together as a boundary with complex impedance. The SRRs oriented in the $x(y)$ direction have three lumped-element parameters R_1 (R_2), L_1 (L_2) and C_1 (C_2). Four segments of semi-infinite transmission lines, having appropriate intrinsic impedances Z_0, are used to mimic the free space through which the light waves propagate. In order to mimic the reversed polarization phenomena for light propagation in the opposite directions of the PCSs, the mutual magnetic inductance is artificially set to be M and $-M$ for waves incident in the +z and −z directions. Basic circuit analysis techniques can be used to derive the transmissions when there are incident waves with x and/or y polarizations. Subsequently, transmissions of circularly polarized waves can then be calculated from the results of two linearly polarized waves (t_{xx}, t_{yx}, t_{yy}, and t_{xy}).[14] Assuming a time dependence of $e^{i\omega t}$, the electric fields of RCP and LCP waves are defined as $E_\pm = (1/\sqrt{2})E_0(\hat{x} \pm i\hat{y})$. By changing the base vectors, the complex transmission coefficients of linear polarizations can be converted into the transmission coefficients of circular polarizations.

$$\begin{pmatrix} t_{++} & t_{--} \\ t_{-+} & t_{+-} \end{pmatrix}$$
$$= \frac{1}{2} \begin{pmatrix} t_{xx} + t_{yy} - i(t_{xy} - t_{yx}) & t_{xx} - t_{yy} + i(t_{xy} + t_{yx}) \\ t_{xx} - t_{yy} - i(t_{xy} + t_{yx}) & t_{xx} + t_{yy} + i(t_{xy} - t_{yx}) \end{pmatrix} \quad (1)$$

Therefore, after some trivial treatment, the asymmetric transmission for an RCP wave is obtained based on the OLE model as follows,

$$\Delta_+ = \left|t_{-+}^{+z}\right|^2 - \left|t_{-+}^{-z}\right|^2 = \frac{2(R_1 - R_2)Z_0^2 M\omega}{|D|^2} \quad (2)$$

Where the denominator D depends on the parameters of all the lumped-elements,

$$D = 2\left[\left(L_1 L_2 - M^2\right)\omega^2 - \left(L_1 R_2 + L_2 R_1\right)i\omega \right.$$
$$- \left(\frac{L_1}{C_2} + \frac{L_2}{C_1} + R_1 R_2\right) + \left(\frac{R_1}{C_2} + \frac{R_2}{C_1}\right)\frac{i}{\omega}$$
$$+ \frac{1}{C_1 C_2 \omega^2} \right] + Z_0\left[\left(\frac{1}{C_1} + \frac{1}{C_2}\right)\frac{i}{\omega}\right.$$
$$- \left(L_1 + L_2\right)i\omega - \left(R_1 + R_2\right) - \frac{Z_0}{2}\right] \quad (3)$$

where $i = \sqrt{-1}$, and ω is the circular frequency of the wave.

waves, since the eigenstates of PCS are elliptically polarized waves. Therefore, the total transmission intensity for RCP or LCP waves incident in the +z direction is $T_\pm^{+z} = \left|t_{\pm\pm}^{+z}\right|^2 + \left|t_{\mp\pm}^{+z}\right|^2$. The superscript '+z' denotes the propagation direction, while t_{++}^{+z} and t_{-+}^{+z} are the transmission amplitude of RCP to RCP and the conversion amplitude of RCP to LCP waves, respectively. Similarly, for circularly polarized waves incident in the −z direction, the total transmission intensity is $T_\pm^{-z} = \left|t_{\pm\pm}^{-z}\right|^2 + \left|t_{\mp\pm}^{-z}\right|^2$.

Materials
Views
www.MaterialsViews.com

ADVANCED
OPTICAL
MATERIALS
www.advopticalmat.de

COMMUNICATION

From Equation (2), one sees that the asymmetric transmission crucially depends on the parameter M, R_1, and R_2. If there is no magnetic coupling effect ($M = 0$) or no loss in the structure ($R_1 = R_2 = 0$), the asymmetric transmission will vanish. Furthermore, even when the structure is lossy and the magnetic coupling effect exists, asymmetric transmission still vanishes under the condition ($R_1 = R_2 \neq 0$). Therefore, being lossy is a necessary condition, but not a sufficient condition, for an anisotropic PCS to show asymmetric transmission. The last conclusion has never been illustrated in previous studies. From Equation (2), it is clear that the magnetic coupling effect M and the anisotropy of loss ($R_1 - R_2$), instead of the whole loss, are crucial for achieving asymmetric transmission for the PCSs of Figure 1a. Therefore, we can manipulate the asymmetric transmission by changing the anisotropy of loss and the magnetic coupling coefficient. Additional discussions on Equations (2) and (3) can be found in Section 1 of the Supporting Information.

In order to see the dependence of the asymmetric transmission on the lumped element parameters in more detail, the numerical calculations of Equation (2) are carried out. However, before that, we need to know the approximate ranges in which the values of the lumped-element parameters (M, R_1, L_1, C_1, etc.) lie. Firstly, by referring to earlier studies,[25,26] we find a typical value of 0.09 for the magnetic coupling coefficient $\kappa = M/\sqrt{L_1 L_2}$. In the OLE model, we have simplified the resonance of the SRRs into electric and magnetic dipoles. However, the real resonant modes of the SRRs (especially SRRs with large sizes) may deviate from that of the ideal dipoles, and this may affect the magnitude of κ. Additionally, κ is also related to the distances between the SRRs. Secondly, for the parameters of R_1, L_1, and C_1, etc., we obtain them by fitting the results of the OLE model to the curves of the simulation results of one set of SRRs. The simulations were performed based on a commercial finite-integration time-domain algorithm, and the details of the simulations can be found in the Supporting Information. From the fitting results (see Section 2 of the Supporting Information), we get typical values of $R = 69\ \Omega$, $L = 7.8 \times 10^{-13}$ H, and $C = 7.5 \times 10^{-19}$ F. Now we are free to adjust the parameters (R_1, L_1, C_1, R_2, L_2, C_2, and κ) in reasonable ranges to see what condition is more suitable to obtain asymmetric transmission for the PCSs.

According to Equations (2) and (3), we numerically calculated the maximum absolute values of asymmetric transmissions in the whole operation frequency range ($|\Delta_+|_{max}$) for different situations. **Figure 2**a shows the results of $|\Delta_+|_{max}$ as a function of different R_1 and R_2 while setting the other parameters as $L_1 = L_2 = 7.8 \times 10^{-13}$ H and $C_1 = C_2 = 7.5 \times 10^{-19}$ F. It is seen that asymmetric transmissions always exist except for on the line of $R_1 = R_2$. This implies that even when the two sets of SRRs have the same inductance and capacitance, asymmetric transmission can still exist as long as symmetry of loss parameters (resistances) are broken. $|\Delta_+|_{max}$ reaches high values near the regions ($R_1 = 0$, $R_2 = 250\ \Omega$) and ($R_1 = 250\ \Omega$, $R_2 = 0$). Figure 2b shows the results of $|\Delta_+|_{max}$ as a function of $\log(L_2/L_1)$ and $\log(C_2/C_1)$ while setting the other two parameters as $R_1 = 69\ \Omega$, $R_2 = 30\ \Omega$, $L_1 = 7.8 \times 10^{-13}$ H and $C_1 = 7.5 \times 10^{-19}$ F. It is clearly seen that $|\Delta_+|_{max}$ reaches the highest value at the point where $\log(L_2/L_1) = 0.36$ and $\log(C_2/C_1) = -0.36$. At this point, the resonance frequencies of the two sets of SRRs are equal and the quality
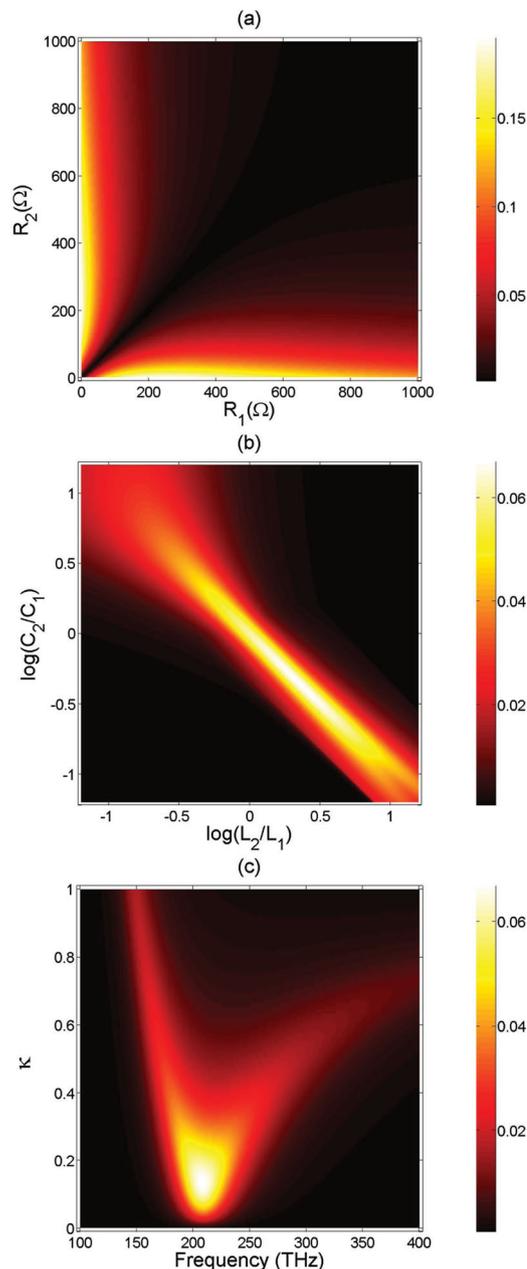

Figure 2. (a) The maximum absolute values of the asymmetric transmissions in the whole operation frequency range ($|\Delta_+|_{max}$) as a function of parameters of R_1 and R_2 while keeping the other parameters as $L_1 = L_2 = 7.8 \times 10^{-13}$ H, $C_1 = C_2 = 7.5 \times 10^{-19}$ F, and $\kappa = 0.09$. (b) The value of $|\Delta_+|_{max}$ as a function of $\log(L_2/L_1)$ and $\log(C_2/C_1)$ while keeping the other parameters as $R_1 = 69\ \Omega$, $R_2 = 30\ \Omega$, $L_1 = 7.8 \times 10^{-13}$ H, $C_1 = 7.5 \times 10^{-19}$ F, and $\kappa = 0.09$. The peak value (0.0674) is at (0.36, –0.36). (c) The value of $|\Delta_+|$ as a function of frequency and the magnetic coupling coefficients κ while keeping the other parameters as $R_1 = 69\ \Omega$, $R_2 = 30\ \Omega$, $L_1 = L_2 = 7.8 \times 10^{-13}$ H, and $C_1 = C_2 = 7.5 \times 10^{-19}$ F.

factors ($Q = X_L / R$) of the two sets of SRRs are also equal. For both Figure 2a and b, the parameter κ is set to be a typical value of 0.09.[25,26] Figure 2c shows the results of $|\Delta_+|$ as a function of frequency and the magnetic coupling coefficients κ while keeping the other parameters as $R_1 = 69\ \Omega$, $R_2 = 30\ \Omega$, $L_1 =$
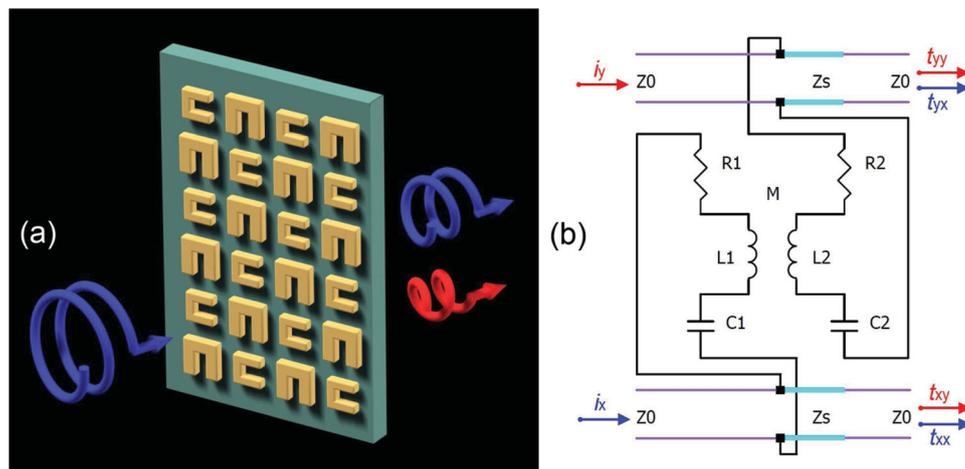
COMMUNICATION

Figure 3. (a) Schematics of the planar chiral structures with a substrate. (b) The corresponding OLE model in which the substrate with impedance Z_s is included.

$L_2 = 7.8 \times 10^{-13}$ H and $C_1 = C_2 = 7.5 \times 10^{-19}$ F. It is seen that the values of $|\Delta_+|$ reaches the maximum when κ is around 0.14. When κ is larger than 0.14, a higher value of κ will result in a lower value of asymmetric transmission. More detailed discussions on the effects of κ on the asymmetric transmission can be found in Section 3 of the Supporting Information.

In order to verify the above theoretical works, we designed and fabricated two PCS samples (Sample I and II) via e-beam lithography and lift-off method. The details of fabrication and measurement procedures can be found in the Experimental Section. For the PCS samples of experiments, due to the existence of the substrate, the corresponding OLE model is a little different from that of Figure 1c. **Figure 3** shows the schematics of the PCS with a substrate and the corresponding OLE model in which we inserted a segment of transmission line with a length of 0.33 mm and impedance of $Z_s = 215.77$ Ω to mimic the function of the sapphire substrate. During the calculations with the OLE model, we first obtain the lumped element parameters by fitting curves to the experimental results of t_{xx}, t_{yy} and t_{yx}. Then, by using these lumped element parameters, we calculate the transmission curves of RCP waves and the asymmetric transmissions.

A scanning electron microscopy (SEM) image of Sample I is shown in **Figure 4**a, which has two sets of SRRs of similar mean resistance (the ratio of the mean resistance of the big SRR to that of the small SRR is approx. 0.9). The SEM image of sample II is shown in **Figure 5**a, which consists of one set of thin SRRs and one set of fat SRRs. Intuitively, the fat SRRs have much smaller mean resistance than that of the thin SRRs. The gold SRRs are fabricated on sapphire substrates. The substrates have a thickness of 0.33 mm and a refractive index of 1.746 at the wavelength of 1.55 μm.[29] The gold SRRs have a thickness of 50 nm. Along with the experiment results, we also did simulations. The bottoms of Figure 4a and 5a show typical unit cells of the structures for the experiments and simulations. The permittivity of the gold in the infrared spectral regime was described by the Drude model with plasma frequency $\omega_p = 1.21 \times 10^{16}$ rad/s, and the damping constant $\omega_c = 6.93 \times 10^{13}$ rad/s.[30] During the simulations, in order to

include the randomly distribution of the dimensions of the fabricated SRRs, a super-cell composed of a 6 × 6 array of SRRs with different sizes was adopted.[31,32] We assumed a Gaussian distribution for the width and length of the area surrounded by the SRRs, and the standard deviations were set to be 15 nm for both the width and length. The averaged sizes of the SRRs can be found in the captions of Figures 4a and 5a. In Section 4 of the Supporting Information, we show the simulation results of the structures with two sets of random sized SRRs compared with that of the structures with two sets of uniform sized SRRs.

All the results of experiments, simulations and OLE models are shown in Figures 4b–e and Figures 5b–e.

Figures 4b and 5b show the transmission curves for t_{xx} and t_{yy}. It is seen that, for each sample, the resonant frequencies of two sets of SRRs differ by approx. 25 THz. Figures 4c and 5c show the transmission curves for RCP incident waves propagating in the +z and −z directions. Figures 4d and 5d show the transmission curves for t_{yx}. Figures 4e and 5e show the asymmetric transmissions for RCP waves. For the purpose of completeness, we also calculated the eigenstates of light waves for the structure of Figure 5a at the frequency of the maximum value of asymmetric transmission. They are indeed two co-rotating elliptical polarization eigenstates[11] (see Figure S5 in Section 5 of the Supporting Information). The lumped element parameters for sample I (Figure 4) are ($R_1 = 201$ Ω, $L_1 = 7.65 \times 10^{-13}$ H, and $C_1 = 7.68 \times 10^{-19}$ F), ($R_2 = 262$ Ω, $L_2 = 7.18 \times 10^{-13}$ H, and $C_2 = 6.37 \times 10^{-19}$ F), and $\kappa = 0.05$. The lumped element parameters for sample II (Figure 5) are ($R_1 = 48$ Ω, $L_1 = 3.38 \times 10^{-13}$ H, and $C_1 = 1.90 \times 10^{-18}$ F), ($R_2 = 146$ Ω, $L_2 = 8.23 \times 10^{-13}$ H, and $C_2 = 6.08 \times 10^{-19}$ F), and $\kappa = 0.07$. From the results shown in Figures 4 and 5, it can be seen that the simulation results are qualitatively in good agreement with the experiment results in the whole frequency range. While for the results based on the OLE model, good agreements with the experimental results are found in the lower frequency ranges (below approx. 240 THz) for the transmission curves of t_{xx}, t_{yy}, (Figures 4b and 5b) and RCP waves (Figures 4c and 5c). The large discrepancies in the higher frequency ranges are mainly due to the existence of higher frequency resonances.[22] Nonetheless, the results of
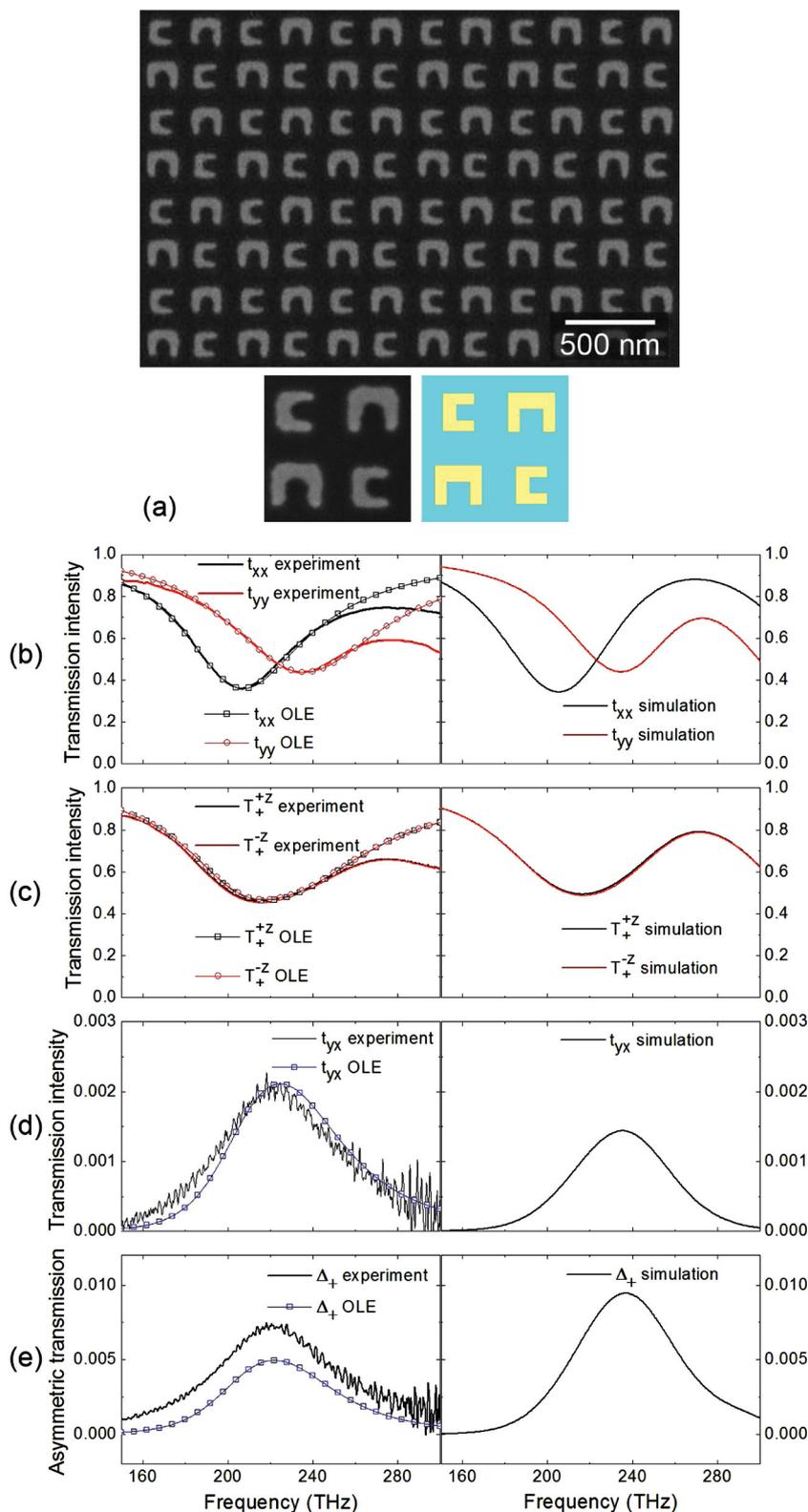
www.MaterialsViews.com

ADVANCED
OPTICAL
MATERIALS
www.advopticalmat.de

COMMUNICATION

Figure 4. (a) Scanning electron microscopy image of the planar chiral structures with similar mean resistances for the two sets of SRRs. The bottom of (a) shows the enlarged views of typical unit cells for experimental and simulation structures. The averaged dimensions for the structure of simulation: $h_1 = 138$ nm, $w_1 = 165$ nm, $h_2 = 110$ nm, $w_2 = 132$ nm, $b_1 = 58$ nm, $m_1 = 43$ nm, $b_2 = 49$ nm, $m_2 = 38$ nm, $t = 50$ nm, and $a_x = a_y = 510$ nm. (b) The spectra of transmission intensity t_{xx} and t_{yy} of experiment and simulation results, and the fitting results to the experimental spectra based on the OLE model. (c) The spectra of transmission intensity of experiment and simulation results for RCP waves, and the calculated results based on the OLE model. (d) The transmission intensity t_{yx} of experiment and simulation results, and the fitting results to the experimental spectra based on the OLE model. (e) The asymmetric transmission intensity Δ_+ of experiment and simulation results for RCP waves, and the calculated results based on the OLE model.

the OLE model are in good agreements with the results of simulations and experiments for the curves of t_{yx} (Figures 4d and 5d) and asymmetric transmissions (Figures 4e and 5e) in the whole frequency range, except for a slight frequency shift. This means that although the higher frequency resonances can dramatically affect the transmission curves of t_{xx}, t_{yy}, and RCP waves in the higher frequency regions, they contribute very little to the results of cross-polarized transmission and asymmetric transmissions in the interested frequency range. In comparing the results of Figure 4e with Figure 5e, it is seen clearly that sample II that is composed of fat and thin SRRs can indeed provide enhanced asymmetry of transmission.

Although it has been stated in previous studies[11–13] that the addition of a substrate has negligible effect on the asymmetric transmission, it is still instructive to have a check. In Section 6 of the Supporting Information, we show the simulation results for the PCS (Samples I and II) with and without a substrate. It is seen that the addition of a substrate can really change a little the magnitude of the asymmetric transmissions, but this small effect does not affect the main arguments of the present report.

It is noteworthy that if higher frequency resonances are included in the OLE model, the agreement between the OLE model and the simulation and experiment results may become better. However, the curve fitting process will require much more effort. In the present report, we only applied the simplest model, and even the simplest model can serve as a good approximation for real structures for the evaluations of asymmetric transmissions. It is noticed that the planar chirality studied in the present report can be regarded as intrinsic structural chirality.[33] Structural two-dimensional chirality can also arise from oblique incidence onto an achiral pattern, and this is called extrinsic structural chirality. It was demonstrated that asymmetric transmission can also be observed for

ADVANCED
OPTICAL
MATERIALS
www.advopticalmat.de

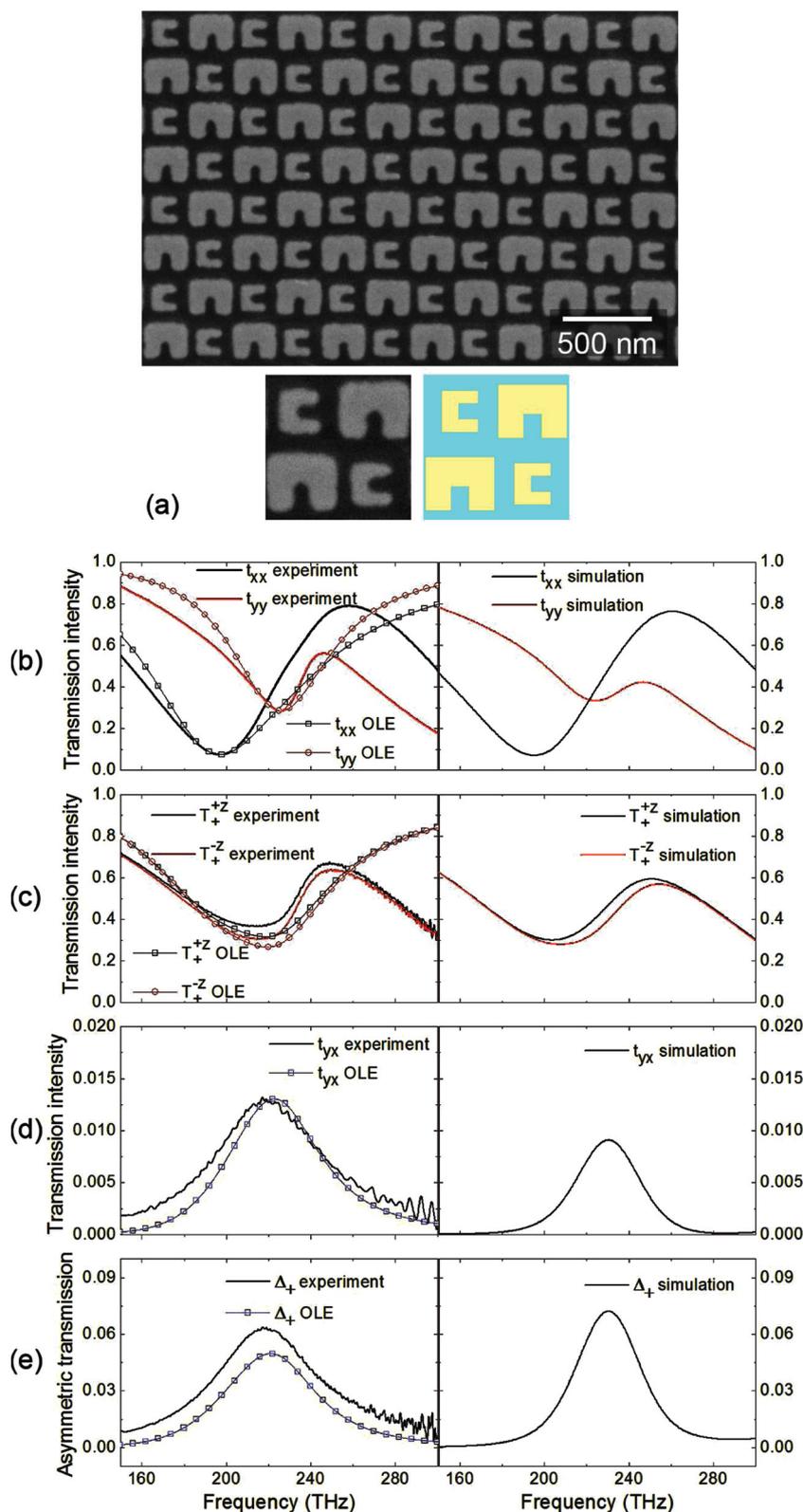Materials
Views
www.MaterialsViews.com

COMMUNICATION

Figure 5. Please see the caption for Figure 4. The dimensions of the PCS structure shown here in (a) are: $h_1 = 189$ nm, $w_1 = 243$ nm, $h_2 = 128$ nm, $w_2 = 146$ nm, $b_1 = 104$ nm, $m_1 = 90$ nm, $b_2 = 59$ nm, $m_2 = 45$ nm, $t = 50$ nm, and $a_x = a_y = 510$ nm.

a lossy structure that shows extrinsic structural chirality. The present study also inspires the investigation of the role of loss in the underlying mechanism of asymmetric transmission that is related to the structures with extrinsic structural chirality.

In conclusion, by using an optical lumped element model, we studied a typical planar chiral structure that shows asymmetric transmissions at infrared frequencies for circularly polarized light waves at normal incidence. The OLE model gave us a deep insight into the physical mechanism of the asymmetric transmission that is related to the planar chiral structures. It is understood that asymmetric transmission of the planar chiral structure is crucially related to the anisotropy of loss. By changing the anisotropy of loss, the asymmetric transmission can be effectively manipulated. Based on the quantitative results of the OLE model, we proposed an optimized planar chiral structure consisting of fat and thin SRRs and obtained an enhanced asymmetry in transmission. Both our simulation and experiment results are in good agreement with the results of the OLE model. The improved understanding of the underlying mechanism of the asymmetric transmission that is related to the anisotropy of loss will apparently benefit future metamaterial designs involving dissipations.

Experimental Section

Structure Fabrication: The planar chiral structures are fabricated via e-beam lithography and lift-off method. After a standard cleaning process, the 0.33 mm-thick sapphire (Al_2O_3) substrate (size 6 mm by 6 mm) was then covered with a 120-nm-thick layer of high resolution positive resist (polymethyl methacrylate) via spin coating. The sample was baked at 180 °C for 90 s, then spin-coated with aquasave and rebaked at 90 °C for 30 s to prevent charging during the next step of e-beam exposure. E-beam lithography was carried out by using Raith's eLiNE nanolithography system. The process of e-beam lithography included the design of the exposure structures and dose tests to find optimum conditions. After e-beam lithography, it was the step of development. The next step was metallization, and the sample was coated with a 50 nm-thick gold film via electron-beam evaporation. The final steps were the lift-off and the inspection by a scanning electron microscope. All structures had a total area of 100×100 µm.

Optical Characterization: Transmission spectra were measured with a Fourier-transform infrared spectrometer (Bruker Vertex 70 V, tungsten lamp) combined with an infrared microscope (Bruker Hyperion 2000, 15× Cassegrain objective, NA = 0.4,

COMMUNICATION

thermoelectric-cooled MCT detector, infrared polarizer). For the data in Figures 3d and 4d, the incident light was circularly polarized by a superachromatic quarter-wave plate, while detection of the transmitted light was polarization insensitive. The measured spectra were normalized with respected to a bare sapphire substrate.

Supporting Information

Supporting Information is available from the Wiley Online Library or from the author.

Acknowledgements

[1] Z. Wang, Y. Chong, J. D. Joannopoulos, M. Soljacic, *Nature* **2009**, *461*, 772.
[2] L. Fan, J. Wang, L. T. Varghese, H. Shen, B. Niu, Y. Xuan, A. M. Weiner, M. Qi, *Science* **2012**, *335*, 447.
[3] Z. Yu, S. Fan, *Nat. Photon.* **2009**, *3*, 91.
[4] C. E. Ruter, K. G. Makris, R. El-Ganainy, D. N. Christodoulides, M. Segev, D. Kip, *Nat. Phys.* **2010**, *6*, 192.
[5] L. Feng, M. Ayache, J. Huang, Y. Xu, M. Lu, Y. Chen, Y. Fainman, A. Scherer, *Science* **2011**, *333*, 729.
[6] A. E. Serebryannikov, E. Ozbay, *Opt. Express* **2009**, *17*, 13335.
[7] C. Menzel, C. Helgert, C. Rockstuhl, E. B. Kley, A. Tunnermann, T. Pertsch, F. Lederer, *Phys. Rev. Lett.* **2010**, *104*, 253902.
[8] S. Cakmakyapan, H. Caglayan, A. E. Serebryannikov, E. Ozbay, *Appl. Phys. Lett.* **2011**, *98*, 051103.
[9] W. Ye, X. Yuan, C. Zeng, *Opt. Lett.* **2011**, *36*, 2842.
[10] J. Hwang, M. H. Song, B. Park, S. Nishimura, T. Toyooka, J. W. WU, Y. Takanishi, K. Ishikawa, H. Takezoe, *Nat. Mater.* **2005**, *4*, 383.
[11] V. A. Fedotov, P. L. Mladyonov, S. L. Prosvirnin, A. V. Rogacheva, Y. Chen, N. I. Zheludev, *Phys. Rev. Lett.* **2006**, *97*, 167401.
[12] V. A. Fedotov, A. S. Schwanecke, N. I. Zheludev, V. V. Khardikov, S. L. Prosvirnin, *Nano lett.* **2007**, *7*, 1996.
[13] A. S. Schwanecke, V. A. Fedotov, V. V. Khardikov, S. L. Prosvirnin, Y. Chen, N. I. Zheludev, *Nano Lett.* **2008**, *8*, 2940.
[14] R. Singh, E. Plum, C. Menzel, C. Rockstuhl, A. K. Azad, R. A. Cheville, F. Lederer, W. Zhang, N. I. Zheludev, *Phys. Rev. B* **2009**, *80*, 153104.
[15] E. Plum, V. A. Fedotov, N. I. Zheludev, *Appl. Phys. Lett.* **2009**, *94*, 131901.
[16] S. V. Zhukovsky, A. V. Novitsky, V. M. Galynsky, *Opt. Lett.* **2009**, *34*, 1988.
[17] C. Menzel, C. Rockstuhl, F. Lederer, *Phys. Rev. A* **2010**, *82*, 053811.
[18] N. Liu, S. Kaiser, H. Giessen, *Adv. Mater.* **2008**, *20*, 4521.
[19] R. Singh, C. Rockstuhl, F. Lederer, W. Zhang, *Phys. Rev. B* **2009**, *79*, 085111.
[20] M. Decker, S. Linden, M. Wegener, *Opt. Lett.* **2009**, *34*, 1579.
[21] J. B. Pendry, A. J. Holden, D. J. Robbins, W. J. Stewart, *IEEE Trans. Microw. Theory Tech.* **1999**, *47*, 2075.
[22] S. Linden, C. Enkrich, M. Wegener, J. Zhou, T. Koschny, C. M. Soukoulis, *Science* **2004**, *306*, 1351.
[23] E. Ozbay, *Science* **2006**, *311*, 189.
[24] V. M. Shalaev, *Nature Photon.* **2007**, *1*, 41.
[25] N. Liu, H. Liu, S. Zhu, H. Giessen, *Nature Photon.* **2009**, *3*, 157.
[26] I. Sersic, M. Frimmer, E. Verhagen, A. F. Koenderink, *Phys. Rev. Lett.* **2009**, *103*, 213902.
[27] A. K. Azad, A. J. Taylor, E. Smirnova, J. F. O'Hara, *Appl. Phys. Lett.* **2008**, *92*, 011119.
[28] Y. Sun, B. Edwards, A. Alu, N. Engheta, *Nat. Mater.* **2012**, *11*, 208.
[29] E. D. Palik, *Handbook of Optical Constants of Solids II*, Academic Press, **1998**.
[30] E. D. Palik, *Handbook of Optical Constants of Solids*, Academic Press, **1998**.
[31] K. B. Alici, A. B. Turhan, C. M. Soukoulis, E. Ozbay, *Opt. Express* **2011**, *19*, 14260.
[32] K. B. Alici, A. E. Serebryannikov, E. Ozbay, *Photon. Nanostruct.* **2011**, *9*, 15.
[33] E. Plum, V. A. Fedotov, N. I. Zheludev, *J. Opt.* **2011**, *13*, 024006.